Estimation of axial compressive strength of unidirectional carbon fiber-reinforced plastic considering the variability of fiber misalignment

Masahito Ueda [a*], Yuki Suzuki [a], and Silvestre T Pinho [b]

[a] Nihon University, 1-8-14 Kanda-surugadai, Chiyoda, Tokyo 101-8308, Japan

[b] Department of Aeronautics, Imperial College London, London, South Kensington, SW7 2AZ, UK

*Corresponding author: ueda.masahito@nihon-u.ac.jp

Abstract

The analytical method to calculate the axial compressive stress-strain relation of a unidirectional carbon fiber-reinforced plastic (UD CFRP) was presented considering the variability of the fiber misalignment angle. Because the compressive load-bearing capability of fibers surrounded by a matrix was different depending on the fiber misalignment angle, fibers were grouped based on the misalignment angle. The contribution to the load bearing was calculated and summed based on the area ratio of the fiber groups. All fibers supported a compressive load in the initial loading. However, with increased loading, the load-bearing capabilities of the different fiber groups decreased more dramatically with greater misalignment angles. The fibers with a misalignment angle of 0.5^{o} showed a large load drop after their maximum loading, which triggered the ultimate failure. The variability of the fiber misalignment angle was indispensable to determining the axial compressive strength under the assumption of zero mean fiber

misalignment angle.

Keywords: Polymer-matrix composites (PMCs), Carbon fibers, Strength, Analytical modelling

1. Introduction

The axial compressive strength of a unidirectional carbon fiber-reinforced plastic (UD CFRP) is lower than the axial tensile strength. The axial tensile strength is determined by the reinforcing fiber, whereas the axial compressive strength is limited by the matrix failure or instability. During compressive loading, fiber waviness causes shear deformation in the matrix, which yields locally and loses its fiber-supporting capability. The broadening of the matrix-yielding zone finally causes the lateral collapse of fibers [1,2].

The fiber waviness occurs during the manufacturing process and is inherent in UD CFRP because of the very small diameter of the carbon fiber [3,4]. Fiber waviness is quantitatively evaluated using the fiber misalignment angle defined in a cross-section [5]. All carbon fibers align to the axial direction of a UD CFRP, although there is some variability due to the waviness. The fiber waviness is, therefore, defined by variability, with a mean fiber misalignment angle of zero.

The axial compressive strength is calculated by considering matrix nonlinear behavior and a fiber misalignment angle [6–8] that is typically assumed to be a constant or equivalent, effectively ignoring the variability in the angle. Furthermore, when the mean fiber misalignment angle is assumed to be zero, unrealistic compressive strength is derived.

In the literature, finite element analysis incorporating fiber waviness is often conducted to simulate

axial compressive failure. Various types of fiber waviness, such as uniform waviness [9,10], localized waviness [11,12], continuously changing waviness [13,14], and random waviness [15,16], were studied. Actual fiber waviness was also modeled based on an X-ray computed tomography technique to develop the digital twin of a UD CFRP, and the axial compressive strength was calculated [17,18]. Numerical methods are effective to calculate the compressive strength considering the arbitrary fiber waviness. However, analytical methods are needed to reveal the mechanics of compressive failure caused by the variability in the fiber misalignment angle.

In this paper, an analytical method that accounts for the variability in the fiber misalignment angle to predict the axial compressive stress-strain relationship and the resulting compressive failure is presented. The mean fiber misalignment angle was assumed to be zero and the effect of the variability on the axial compressive strength was studied. The combined effect of the variability and the mean fiber misalignment angle was also clarified. Kink-band width was estimated by considering the local fiber kinking mode. The scenario of the axial compressive failure caused by the variability of the fiber misalignment angle was discussed based on the analytical method.

2. Analysis of axial compressive stress-strain response

2.1 UD CFRP with a single fiber misalignment angle

Uniaxial compression is applied to the fiber direction of a UD CFRP as shown in Fig. 1. The *x*- and *y*-axes are the loading direction and the transverse direction, respectively. The nominal fiber direction corresponds to the x-axis, although the fibers have some misalignment developed during the

manufacturing. The 1- and 2-axes are the local fiber and the transverse directions, respectively.

Axial compressive loading develops longitudinal shear stress τ_{12} and strain γ_{12} due to the fiber misalignment angle ϕ_0. The fiber angle $\phi\,(=\phi_0+\gamma_{12})$ increases as the axial compressive loading increases [18–20]. The axial compressive stress σ_x is related to the longitudinal shear stress according to Eq. (1) [6–8]:

$$\sigma_x \approx \frac{\tau_{12}}{(\phi_0+\gamma_{12})}. \tag{1}$$

σ_x is calculated by substituting a value of τ_{12} and the corresponding γ_{12} obtained from the shear stress-strain curve of a UD CFRP and assuming a constant ϕ_0. The maximum value of σ_x gives the axial compressive strength. The graphical expression of Eq. (1) gives a clear guideline to improve the compressive strength of a UD CFRP in terms of nonlinear shear property and fiber misalignment angle [8]. However, the variability in the fiber misalignment angle is not taken into account. Furthermore, the equation gives an elastic shear instability solution when ϕ_0=0°and the compressive strength is equal to the longitudinal shear modulus G_{12} [21].

The compressive strength corresponds to the fiber kinking stress in the case of the global fiber kinking mode in which the kink-band width is as long as the specimen length. However, global fiber kinking is an unrealistic mode because it requires uniform shear stress development throughout the specimen. Local fiber kinking is a dominant mode in the actual composite because of nonuniform shear stress due to the variability in fiber misalignment. Fiber kinking is localized and the resultant kink-band width is about 50–

200 μm [22]. In the local fiber kinking mode, the compressive strength does not correspond to the fiber kinking stress. Fiber kinking is developed after the maximum loading as a post-failure when the bifurcation condition is satisfied [23], which is explained in Section 2.3.

The axial Young's modulus of a UD CFRP E_x is reduced according to an increase of the fiber angle ϕ (= $\phi_0 + \gamma_{12}$) [24]:

$$\frac{1}{E_x} = \frac{1}{E_{11}} + \frac{1}{E_{22}}(\phi_0 + \gamma_{12})^4 + \left(\frac{1}{G'_{12}} - \frac{2\nu_{12}}{E_{11}}\right)(\phi_0 + \gamma_{12})^2, \quad (2)$$

where E_{11} and E_{22} are the fiber directional and the transverse Young's modulus, ν_{12} is Poisson's ratio, and G'_{12} (=$d\tau_{12}/d\gamma_{12}$) is the tangent shear modulus. E_{11}, E_{22}, and ν_{12} are assumed to be constant irrespective of longitudinal shear strain γ_{12}. However, G_{12} is reduced with an increase of γ_{12} because of matrix plasticity. Thus, G_{12} is replaced by G'_{12}. E_x is also expressed as a function of γ_{12} just as σ_x.

Axial compressive strain ε_x under the uniaxial compression is obtained as:

$$\varepsilon_x = \frac{\sigma_x}{E_x}. \quad (3)$$

2.2 UD CFRP with variability in fiber misalignment angle

Each fiber in a UD CFRP has individual waviness [17–20]. The fiber misalignment angle ϕ_0 varies typically within a maximum of ±3° in the cross-section of a UD CFRP produced from a prepreg sheet [25]. The fiber misalignment angle cannot be determined as a single value because of its variability. The variability is often assumed to follow a normal distribution of mean fiber misalignment angle $\bar{\phi}_0$ and standard deviation Σ, as shown in Fig. 2(a) [5,14,25]. The probability density function of the fiber angle is given in Eq. (4):

$$f(\phi_0) = \frac{1}{\sqrt{2\pi\Sigma^2}} exp\left(-\frac{(\phi_0 - \bar{\phi}_0)^2}{2\Sigma^2}\right). \quad (4)$$

In this study, fibers with the surrounding matrix are divided into several groups based on the fiber misalignment angle to calculate the compressive load sharing (see example Fig. 2b). A fiber group θ_0^i is defined by fibers with a misalignment angle between ϕ_0^i and ϕ_0^{i+1} ($\phi_0^i < \phi_0^{i+1}$). The existing probability A^i of the fiber group θ_0^i is calculated as:

$$A^i(\theta_0^i) = P\left(\phi_0 \le \phi_0^{i+1}\right) - P\left(\phi_0 \le \phi_0^i\right)$$
$$= \int_{\phi_0^i}^{\phi_0^{i+1}} f(\phi_0)\, d\phi_0, \quad (5)$$

where $\theta_0^i (= \frac{\phi_0^{i+1} + \phi_0^i}{2})$ is a representative fiber group angle and $P(\cdot)$ is probability. The existing probability is equal to the area ratio of the fiber group area to the whole cross-sectional area of the UD CFRP. The fiber group area includes the matrix around the fibers.

Eq. (1) indicates that the fiber misalignment angle ϕ_0 affects the compressive behavior. The axial compressive stress is not uniform within the composite, but varies depending on the local fiber misalignment angle. Thus, assuming that fiber groups with different misalignments are arranged in parallel, the axial compressive stress of a UD CFRP calculated including the variability of the fiber misalignment angle is obtained by summing the shared load by every fiber group as:

$$\bar{\sigma}_x = \sum_i \sigma_x^i A^i, \quad (6)$$

where $\sigma_x^i (= \tau_{12}/\left(\theta_0^i + \gamma_{12}\right))$ is the compressive stress of the fiber group θ_0^i. The summation needs to be done under the same axial compressive strain condition because of the rule of mixture for parallel fibers.

The tangent shear modulus is also obtained using the area ratio of each fiber group θ_0^i according to Eq. (7):

$$\bar{G}'_{12} = \frac{1}{\sum_i \frac{A^i}{G_{12}^{i\prime}}}. \tag{7}$$

2.3 Fiber kinking stress

The compressive stress $\bar{\sigma}_{cr}$ of a UD CFRP to initiate fiber kinking is expressed as follows [21,26]:

$$\bar{\sigma}_{cr} = \bar{G}'_{12} + \frac{\pi^2 V_f^{2D} E_f}{12}\left(\frac{d_f}{w}\right)^2, \tag{8}$$

where V_f^{2D} is a two-dimensional equivalent fiber volume fraction [1], E_f is the Young's modulus of the fiber, d_f is the fiber diameter, and w is the half-wavelength of fiber bending deformation. w is approximately the same as the kink-band width. ~~T~~The derivation of Eq. (8) ~~is~~ shown in Appendix. When the axial compressive stress has reached the fiber kinking stress, the bifurcation condition is satisfied, and local fiber kinking develops. The matrix yielding, i.e., the reduction of G'_{12}, starts in a small zone, the length of which corresponds with w, and broadens along the fiber direction with an increase in axial compressive load [1,2,17]. The fiber kinking stress decreases with an increase of w. The bifurcation point can be determined by a tangent point between the axial compressive stress curve (Eq. 1) and the fiber kinking stress curve (Eq. 8) by gradually increasing w [23]. The bifurcation point always occurs after the maximum loading, and the kink band is formed at post-failure.

3. Experimental

3.1 Materials

Angle-ply and unidirectional CFRPs were fabricated from polyacrylonitrile-based carbon fiber and epoxy resin. A prepreg sheet (T800S/#2592, Toray Industries) was laminated and consolidated in an oven under vacuum. The ply thickness of the prepreg sheet was 0.1mm. Material properties are shown in Table 1.

3.2 In-plane shear test on angle-ply CFRP

The in-plane shear test on the angle-ply CFRP was performed to obtain the longitudinal shear stress-strain curve. The angle-ply laminate of $[\pm 45]_{5S}$ was prepared. The specimen was 250 mm in length, 25 mm in width, and 2 mm in thickness. End tabs were attached to both ends of the specimen, and the resultant gauge length was 150 mm. A biaxial strain gauge was attached to the face of the specimen. A universal testing machine (AG-IS 150kN, Shimadzu Corp.) was used at a testing speed of 3.0 mm/min. A total of five specimens were prepared and tested.

3.3 Axial compression test on UD CFRP

The axial compression test on the UD CFRP was performed to obtain the compressive stress-strain curve. The unidirectional laminate of $[0]_{10}$ was prepared. The specimen was 78 mm in length, 12.5 mm in width, and 1 mm in thickness. End tabs were attached to both ends of the specimen, and the resultant gauge length was 8 mm. Two strain gauges were attached to the front and back faces of the specimen, and their average value was taken as the applied strain. A universal testing machine (AG-IS 150kN, Shimadzu Corp.) was used at a testing speed of 1.0 mm/min. A total of five specimens were prepared and tested.

4. Results and discussion

4.1 Experimental longitudinal shear and axial compression behavior

The experimental longitudinal shear stress-strain curves obtained from the in-plane shear tests on the angle-ply CFRP are shown in Fig. 3(a). The Ramberg–Osgood equation was used to approximate the relationships.

The experimental axial compressive stress-strain curves obtained from the axial compression tests on the UD CFRP are shown in Fig. 3(b). The average compressive strength and failure strain were 1453 MPa and 0.0092, respectively.

4.2 Analytical axial compressive stress-strain curve

σ_x and ε_x were calculated by Eq. (1) and Eq. (3) using the experimental longitudinal shear stress-strain curve of the Ramberg–Osgood equation in Fig. 3(a). The analytical axial compressive stress-strain curves were calculated with every 0.1º of the fiber misalignment angle (ϕ_0=0°, ±0.1º, ±0.2º, …, ±5.0º) assuming uniform fiber misalignment angle and are shown in Fig. 4(a). Some curves are not shown due to space limitations. All calculations in this paper were done by spreadsheet software (Excel, Microsoft Corp.) except for the interpolation of axial compressive stress and tangent shear modulus to make identical summation points regarding axial compressive stress.

Fiber groups successively lowered their load-bearing capability in descending order of the misalignment angle with an increase in compressive loading. The fiber groups with large ϕ_0 showed a gradual load decrease after maximum loading. In contrast, the fiber groups with small ϕ_0 were more prone to fail catastrophically, showing snap-through behaviors after maximum loading because E_x

decreased quickly along with G'_{12}. The fiber group with ϕ_0=0° carried the axial compressive load linearly up to the fiber crush stress [22] or the critical stress of elastic shear instability (σ_{cr}=G_{12}).

The mean fiber misalignment angle and standard deviation were assumed to be $\bar{\phi}_0$ =0° and Σ=0.6°, following the report on prepreg-based CFRP [25]. Representative fiber group angles were segmented every 0.1º (θ_0^i=0, ±0.1, ±0.2, …, ±5.0º) to calculate the area ratio. Each stress-strain curve in Fig. 4(a) was scaled by multiplying the area ratio to obtain a shared load. Stress-strain curves (colored curves) in Fig. 4(b) indicate load sharing by the fiber groups with different misalignment angle. Here, the strain reduction due to snap-through behavior does not happen due to load sharing by other fiber groups. The axial compressive loads supported by fibers were different, depending on the misalignment angles. The resultant axial compressive stress was obtained by summing every shared load and is shown in the bold black curve in Fig. 4(b). Each scaled axial compressive stress-strain curve was interpolated employing a Python code so that the stresses were summed at the corresponding strain points.

The analytical axial compressive stress-strain curve showed an almost linear region during the initial loading. Fiber groups with large misalignment angles successively decreased their load-bearing capability in descending order of the misalignment angle with an increase in compressive loading. The load still increased because of the small load sharing of the fiber groups with large misalignment angles, which indicated that the large fiber misalignment angle did not trigger the ultimate failure [27]. However, the slope started to decrease when approaching the maximum loading. The curve became flat when the fiber group with the representative angle of 0.5º reached the peak loading. The fiber group triggered the

ultimate failure of the UD CFRP, although fiber groups with misalignment angles less than 0.5º still carried more compressive load. Fibers with a misalignment angle larger than ±0.5º were about 60%, and those fibers degraded the load-bearing capability before peak loading due to matrix yielding. The failure strain of the fiber groups with a representative angle of ≈0.5º is 0.0092, which agrees with the experimental compressive failure strain. The axial compressive strength was 1307 MPa, which is 10% smaller than the experimental result, as will be discussed in Section 4.3. Compressive strength was obtained even on the assumption of $\bar{\phi}_0$= 0° because of the variability of fiber misalignment.

The stress-strain curve was serrated after maximum loading because of large load drops of fiber groups with smaller misalignment angles. More precise discretization by increasing the precision of θ_0^i results in a smooth post-failure curve.

The normal distribution was used to calculate the axial compressive stress-strain curve in this study. A measured distribution of the fiber misalignment angle, which does not follow the normal distribution, is also used for the calculation of the analytical stress-strain curve.

4.3 Effect of the variability of fiber misalignment angle on the axial compressive strength

Analytical stress-strain curves were calculated assuming a zero mean fiber misalignment angle $\bar{\phi}_0$ = 0° and different standard deviations Σ= 0.2, 0.4, 0.6, 0.8, and 1.0°, as shown in Fig. 5(a). The maximum fiber misalignment angle was almost within ±3°. The analytical axial compressive stress-strain curves are shown in Fig. 5(b) with the experimental curves. The compressive strength increased with the decrease in the standard deviation. The estimated compressive strengths were 1503, 1422, 1307, 1206, and 1123MPa

for ($\bar{\phi}_0$, Σ) = (0, 0.2), (0, 0.4), (0, 0.6), (0, 0.8), and (0, 1.0) supposing that failure strain was ε_x=0.0092. The analytical compressive strength for ($\bar{\phi}_0$, Σ) = (0, 0.4) agreed well with the experimental result. In the case of ($\bar{\phi}_0$, Σ) = (0, 0.2), reduction of the slope was prevented, and the failure strain could be higher than 0.0092. More precise discretization of the fiber group angle was required to estimate compressive strength when the standard deviation was small. However, such a very small variation has not been reported, and the more precise discretization was omitted in this paper.

The experimental axial compressive stress-strain curve was almost linear up to the ultimate failure, although the analytical curve showed a decrease of slope just before the ultimate failure. The calculated compressive strain was a local strain at which deformation increased locally. In the experiment, the averaged macroscopic strain was measured by strain gauges of 1 mm in length. The strain gauge did not capture the local strain increase, and the local reduction of slope was not measured.

Analytical stress-strain curves were also calculated assuming constant standard deviation Σ = 0.6° and different mean fiber misalignment angles $\bar{\phi}_0$ = 0, 0.2, 0.4, 0.6, 0.8, and 1.0°, as shown in Fig. 6(a). The analytical stress-strain curves are shown in Fig. 6(b) with the experimental curves. The compressive strength increased with the decrease of the mean fiber misalignment angle.

The effect of the mean fiber misalignment angle and the standard deviation on the axial compressive strength was summarized in Fig. 7. Dotted line indicates the axial compressive strength in the case of uniform fiber misalignment angle (standard deviation Σ = 0°), which corresponds to the maximum stresses (indicated by circles) in Fig. 4(a). The solid lines indicate the axial compressive strength in the

cases of Σ = 0.4, 0.6, 0.8, and 1.0°. The standard deviation did not affect the axial compressive strength when the mean fiber misalignment angle was larger than 1.0°. In contrast, the axial compressive strength was strongly degraded by the standard deviation when the mean fiber misalignment angle was less than 1.0°. The mean fiber misalignment angle is zero ($\bar{\phi}_0$= 0) for a UD CFRP; thus, the variation in the fiber misalignment plays an important role in determining the axial compressive strength.

4.4 Kink-band width

Fiber kinking is developed after the maximum loading when the axial compressive stress coincides with the fiber kinking stress [23]. The bifurcation point is determined by gradually decreasing fiber kinking stress by increasing the kink-band width w in Eq. (8) to find a tangent point to the axial compressive stress curve. Fiber kinking stress was overlaid on the compressive stress-strain curves of ($\bar{\phi}_0$, Σ) = (0, 0.4) and (0, 1.0), as shown in Fig. 8. Here, the tangent shear modulus-axial compressive strain curves were interpolated employing a Python code so that the tangent shear modulus was summed at the corresponding strain points to obtain the weighted mean by Eq. (7). Because the stress-strain curve was serrated after maximum loading, the bifurcation point for fiber kinking was roughly identified by finding the corresponding stress. The kink-band width was 60 μm (=12d_f) for ($\bar{\phi}_0$, Σ) = (0, 0.4) and 75 μm (=15d_f) for ($\bar{\phi}_0$, Σ) = (0, 1.0). The kink-band width decreased with a decrease in the standard deviation of the fiber misalignment angle. The small standard deviation caused a high compressive strength, resulting in a narrow kink-band width.

5. Conclusions

Axial compressive stress-strain curves of a UD CFRP were analytically derived based on the longitudinal shear property and the variability in the fiber misalignment angle. The variability was assumed to follow a normal distribution in a cross-section, and the effects of the mean and the standard deviation on the axial compressive strength were revealed. The mean fiber misalignment angle and the standard deviation were ranged $\bar{\phi}_0$= 0~1.0° and Σ= 0.2~1.0° for a prepreg-based UD CFRP. The results obtained in this paper are summarized as follows.

1. The analytical axial compressive stress-strain curve showed an almost linear increase in the initial loading, and the slope decreased just before maximum loading. The reduction of the slope was caused by successive failure of the load-bearing capability of the fibers in descending order of the misalignment angle with an increase in compressive loading.
2. The axial compressive strength was obtained on the assumption of a zero mean fiber misalignment angle of a UD CFRP. The variability of the fiber misalignment angle was indispensable to determining the axial compressive strength. The increased mean fiber misalignment angle further degraded the axial compressive strength.
3. A compressive failure was triggered by the fibers with a misalignment angle of $\bar{\phi}_0$=0.5° due to a relatively large load drop developed by the fibers. The fibers with $\bar{\phi}_0$=0.5° played a key role in the determination of the axial compressive strength.
4. The variability of the fiber misalignment angle strongly degraded the axial compressive strength when the mean fiber misalignment angle was less than 1.0°. In contrast, the effect of the variability

on the axial compressive strength became negligible when the mean fiber misalignment angle was larger than 1.0°.

5. The kink-band width decreased with a decrease in the standard deviation of the fiber misalignment angle. The small standard deviation caused a high compressive strength resulting in a narrow kink-band width.

Acknowledgment

This work was supported by JSPS KAKENHI Grant Number 20K04184.

Appendix. Fiber kinking critical stress

Fiber kinking is developed after the maximum loading as a post-failure when the bifurcation condition is satisfied. When the axial compressive stress σ_x reaches the fiber kinking critical stress σ_{cr}, the UD CFRP snaps from Fig. 1 into Fig. A1 to form fiber kinking. Fiber bending and matrix shear deformation are supposed during the development of fiber kinking. The unit thickness is supposed for the model. Fiber kinking develops without load increase, thus $\sigma_x = \sigma_{cr}$ keeps constant during the deformation. σ_{11} and τ_{12} are also constant. The deflection of fibers due to the kinking is expressed as

$$v = \frac{A}{2} cos \frac{X\pi}{w}. \tag{A1}$$

where A is the amplitude of the deflection, w is the kink-band width, and X is the local fiber direction which coincides with the 1-axis. The shear strain of the matrix is a function of the local fiber direction [1, 21].

$$\gamma_m = \frac{dv}{dX} + \frac{du}{dY} = \left(1 + \frac{d_f}{d_m}\right)\frac{dv}{dX} = -\left(1 + \frac{d_f}{d_m}\right)\frac{A\pi}{2w} sin \frac{X\pi}{w} \tag{A2}$$

Contraction e along the local fiber direction due to the fiber kinking is obtained as follows supposing

dv/dX is small.

$$e = \int ds = \int \left\{1 + \frac{1}{2}\left(\frac{dv}{dX}\right)^2\right\} dX = \frac{A^2\pi^2}{16w} \tag{A3}$$

σ_{11} and τ_{12} is developed by σ_x due to fiber misalignment. The work Π_p done by the σ_{11} and τ_{12} is expressed as follows.

$$\Pi_p = \sigma_{11}(d_f + d_m)e + \tau_{12}(d_f + d_m)A = \sigma_{cr}(d_f + d_m)e + \tau_{m_cr} d_m \frac{A}{1 - V_f} \tag{A4}$$

where d_f and d_m are fiber diameter and distance between adjacent fibers (matrix area), τ_{m_cr} is the matrix shear stress at fiber kinking. Matrix shear stress $\tau_m$is equal to the composite longitudinal shear stress τ_{12} due to the equilibrium condition.

Strain energy due to the matrix shear deformation Π_{ms} is expressed as follows supposing that tangent shear modulus G'_m is constant throughout the width w.

$$\Pi_{ms} = \int_0^w \left(\int_0^{\gamma_m} \tau_m \, d\gamma_m\right) dX \cdot d_m = \left[\int_0^w \Pi_{ms1} dX + \int_0^w \Pi_{ms2} dX\right] d_m \tag{A5}$$

Here,

$$\int_0^w \Pi_{ms1} dX = \int_0^w \left(\frac{G'_m \gamma_m{}^2}{2}\right) dX = \frac{G'_m A^2 \pi^2}{16w}\left(1 + \frac{d_f}{d_m}\right)^2 \tag{A6}$$

$$\int_0^w \Pi_{ms2} dX = \int_0^w \tau_{m_cr}\gamma_m \, dX = \tau_{m_cr} \frac{A}{(1 - V_f)}. \tag{A7}$$

Strain energy due to the fiber bending deformation Π_{fb} is expressed as

$$\Pi_{fb} = \int_0^w \frac{M^2}{2E_f I_f} dx = \frac{E_f I_f}{2} \int_0^w \left(\frac{d^2 v}{dX^2}\right)^2 dX = \frac{E_f}{16}\frac{d_f{}^3}{12}\frac{A^2\pi^4}{w^3}, \tag{A8}$$

where M is the bending moment in the fiber and I_f (=$d_f{}^3/12$) is the second moment of the area.

The following equation is satisfied.

$$\Pi_p = \Pi_{ms} + \Pi_{fb} \tag{A9}$$

Thus, fiber kinking critical stress is obtained.

$$\sigma_{cr} = \frac{G'_m}{(1 - V_f)} + \frac{\pi^2 V_f E_f}{12}\left(\frac{d_f}{w}\right)^2 \tag{A10}$$

Eq. (A10) indicates the local fiber kinking mode with finite kink-band width w. It is noted that the

minimization of the total potential energy $\Pi = \Pi_{ms} + \Pi_{fb} - \Pi_p$ with respect to w i.e., $\partial\Pi/\partial w = 0$ derives infinite kink-band width, by which fiber bending term in Eq. (A10) vanishes. This indicates global fiber kinking mode.

References

[1] S. Pimenta, R. Gutkin, S.T. Pinho, P. Robinson, A micromechanical model for kink-band formation: Part II—Analytical modelling, Composites Science and Technology. 69 (2009) 956–964. https://doi.org/10.1016/j.compscitech.2009.02.003.

[2] P. Davidson, A.M. Waas, Mechanics of kinking in fiber-reinforced composites under compressive loading, Mathematics and Mechanics of Solids. 21 (2016) 667–684. https://doi.org/10.1177/1081286514535422.

[3] M.J. Emerson, K.M. Jespersen, A.B. Dahl, K. Conradsen, L.P. Mikkelsen, Individual fibre segmentation from 3D X-ray computed tomography for characterising the fibre orientation in unidirectional composite materials, Composites Part A: Applied Science and Manufacturing. 97 (2017) 83–92. https://doi.org/10.1016/j.compositesa.2016.12.028.

[4] K. Iizuka, M. Ueda, T. Takahashi, A. Yoshimura, M. Nakayama, Development of a three-dimensional finite element model for a unidirectional carbon fiber reinforced plastic based on X-ray computed tomography images and the numerical simulation on compression, Advanced Composite Materials. 28 (2019) 73–85. https://doi.org/10.1080/09243046.2018.1434731.

[5] S.W. Yurgartis, Measurement of small angle fiber misalignments in continuous fiber composites, Composites Science and Technology. 30 (1987) 279–293. https://doi.org/10.1016/0266-3538(87)90016-9.

[6] M.R. Wisnom, The effect of fibre misalignment on the compressive strength of unidirectional carbon fibre/epoxy, Composites. 21 (1990) 403–407. https://doi.org/10.1016/0010-4361(90)90438-3.

[7] B. Budiansky, N.A. Fleck, Compressive failure of fibre composites, Journal of the Mechanics and Physics of Solids. 41 (1993) 183–211. https://doi.org/10.1016/0022-5096(93)90068-Q.

[8] I.M. Daniel, H.-M. Hsiao, S.-C. Wooh, Failure mechanisms in thick composites under compressive loading, Composites Part B: Engineering. 27 (1996) 543–552. https://doi.org/10.1016/1359-8368(95)00010-0.

[9] S. Kyriakides, R. Arseculeratne, E.J. Perry, K.M. Liechti, On the compressive failure of fiber reinforced composites, International Journal of Solids and Structures. 32 (1995) 689–738. https://doi.org/10.1016/0020-7683(94)00157-R.

[10] F. Naya, M. Herráez, C.S. Lopes, C. González, S. Van Der Veen, F. Pons, Computational micromechanics of fiber kinking in unidirectional FRP under different environmental conditions,

Composites Science and Technology. 144 (2017) 26–35. https://doi.org/10.1016/j.compscitech.2017.03.014.

[11] T.J. Vogler, On the initiation and growth of kink bands in ®ber composites. Part II: analysis, International Journal of Solids and Structures. (2001).

[12] S. Pimenta, R. Gutkin, S.T. Pinho, P. Robinson, A micromechanical model for kink-band formation: Part I — Experimental study and numerical modelling, Composites Science and Technology. 69 (2009) 948–955. https://doi.org/10.1016/j.compscitech.2009.02.010.

[13] M. Romanowicz, Initiation of kink bands from regions of higher misalignment in carbon fiber-reinforced polymers, Journal of Composite Materials. 48 (2014) 2387–2399. https://doi.org/10.1177/0021998313498106.

[14] T. Takahashi, M. Ueda, K. Miyoshi, A. Todoroki, Initiation and propagation of fiber kinking from fiber undulation in a unidirectional carbon fiber reinforced plastic, Composites Part C: Open Access. 3 (2020) 100056. https://doi.org/10.1016/j.jcomc.2020.100056.

[15] M. Bishara, R. Rolfes, O. Allix, Revealing complex aspects of compressive failure of polymer composites – Part I: Fiber kinking at microscale, Composite Structures. 169 (2017) 105–115. https://doi.org/10.1016/j.compstruct.2016.10.092.

[16] Q. Sun, H. Guo, G. Zhou, Z. Meng, Z. Chen, H. Kang, S. Keten, X. Su, Experimental and computational analysis of failure mechanisms in unidirectional carbon fiber reinforced polymer laminates under longitudinal compression loading, Composite Structures. 203 (2018) 335–348. https://doi.org/10.1016/j.compstruct.2018.06.028.

[17] T. Takahashi, M. Ueda, K. Iizuka, A. Yoshimura, T. Yokozeki, Simulation on kink-band formation during axial compression of a unidirectional carbon fiber-reinforced plastic constructed by X-ray computed tomography images, Advanced Composite Materials. 28 (2019) 347–363. https://doi.org/10.1080/09243046.2018.1555387.

[18] T. Takahashi, A. Todoroki, C. Kawamura, R. Higuchi, T. Sugiyama, T. Miyanaga, K. Hattori, M. Ueda, T. Yokozeki, M. Honda, Unidirectional CFRP kinking under uniaxial compression modeled using synchrotron radiation computed tomography imaging, Composite Structures. 289 (2022) 115458. https://doi.org/10.1016/j.compstruct.2022.115458.

[19] M.J. Emerson, Y. Wang, P.J. Withers, K. Conradsen, A.B. Dahl, V.A. Dahl, Quantifying fibre reorientation during axial compression of a composite through time-lapse X-ray imaging and individual fibre tracking, Composites Science and Technology. 168 (2018) 47–54. https://doi.org/10.1016/j.compscitech.2018.08.028.

[20] Y. Wang, M.J. Emerson, K. Conradsen, A.B. Dahl, V.A. Dahl, E. Maire, P.J. Withers, Evolution of fibre deflection leading to kink-band formation in unidirectional glass fibre/epoxy composite under axial compression, Composites Science and Technology. 213 (2021) 108929. https://doi.org/10.1016/j.compscitech.2021.108929.

[21] N.F. Dow, B.W. Rosen, Evaluations of filament-reinforced composites for aerospace structural

applications, NASA Contractor Report. NASA-CR-207 (1965).
[22] T.K. Jeong, M. Ueda, Longitudinal Compressive Failure of Multiple-Fiber Model Composites for a Unidirectional Carbon Fiber Reinforced Plastic, OJCM. 06 (2016) 8–17. https://doi.org/10.4236/ojcm.2016.61002.
[23] M. Ueda, Y. Tasaki, C. Kawamura, K. Nishida, M. Honda, K. Hattori, T. Miyanaga, T. Sugiyama, Estimation of axial compressive strength of unidirectional carbon fiber reinforced plastic considering local fiber kinking, Composites Part C: Open Access. 6 (2021) 100180. https://doi.org/10.1016/j.jcomc.2021.100180.
[24] P.K. Mallick, Fiber-Reinforced Composites: Materials, Manufacturing, and Design, Third Edition, 0 ed., CRC Press, 2007. https://doi.org/10.1201/9781420005981.
[25] T. Yokozeki, T. Ogasawara, T. Ishikawa, Nonlinear behavior and compressive strength of unidirectional and multidirectional carbon fiber composite laminates, Composites Part A: Applied Science and Manufacturing. 37 (2006) 2069–2079. https://doi.org/10.1016/j.compositesa.2005.12.004.
[26] J.G. Haberle, F.L. Matthews, A Micromechanics Model for Compressive Failure of Unidirectional Fibre-Reinforced Plastics, Journal of Composite Materials. 28 (1994) 1618–1639. https://doi.org/10.1177/002199839402801701.
[27] M. Ueda, K. Mimura, T.-K. Jeong, In situ observation of kink-band formation in a unidirectional carbon fiber reinforced plastic by X-ray computed tomography imaging, Advanced Composite Materials. 25 (2016) 31–43. https://doi.org/10.1080/09243046.2014.973173.

Figure legends

Figure 1. Stresses due to local fiber misalignment in a UD CFRP under uniaxial compression.

Figure 2. Variability of fiber misalignment angle. (a) Probability density function. (b) Probability of fiber misalignment angle.

Figure 3. Experimental mechanical response of UD CFRP (T800S/#2592). (a) Longitudinal shear stress-strain curves. (b) Axial compressive stress-strain curves. The coefficients of variation are shown in parentheses.

Figure 4. Analytical axial compressive stress-strain curves. (a) Stress-strain curves assuming uniform

fiber misalignment angle. (b) Scaled stress-strain curves by using the area ratio and the resultant stress-strain curve of $\bar{\phi}_0 = 0^\circ$ and $\Sigma = 0.6^\circ$.

Figure 5. The effect of variability (standard deviation) of fiber misalignment angle. (a) Probability density functions. (b) Axial compressive stress-strain curves.

Figure 6. The effect of mean fiber misalignment angle. (a) Probability density functions. (b) Axial compressive stress-strain curves.

Figure 7. The combined effect of variability (standard deviation) and mean fiber misalignment angle on the axial compressive strength.

Figure 8. Determination of fiber kinking critical stress and kink-band width.

Table 1. Material properties used in the calculation of axial compressive behavior.

Figure A1 Fiber kinking deformation. (a) Deformed shape before and after fiber kinking. The non-kinked shape is shown in light gray. (b) Strain energy of matrix per unit volume due to shear deformation

Figure 1 Stresses due to local fiber misalignment in a UD CFRP under uniaxial compression.

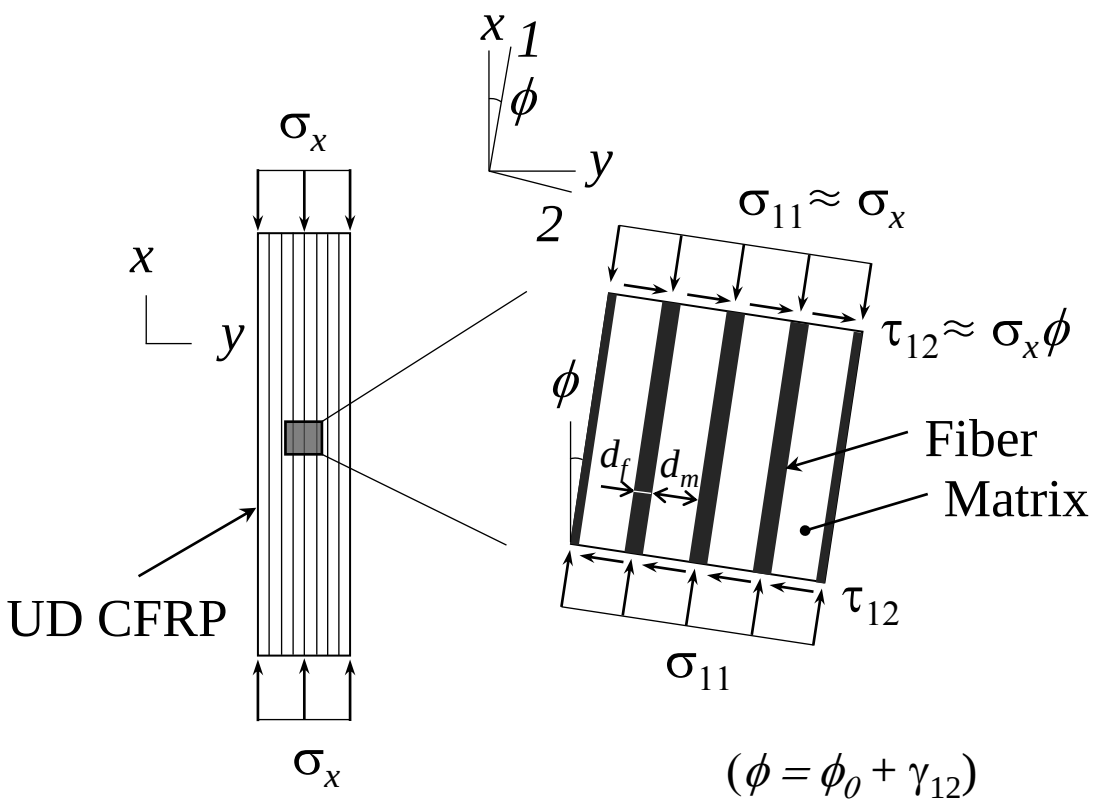

Figure 2 Variability of fiber misalignment angle.
(a) Probability density function (b) Probability of fiber misalignment angle.

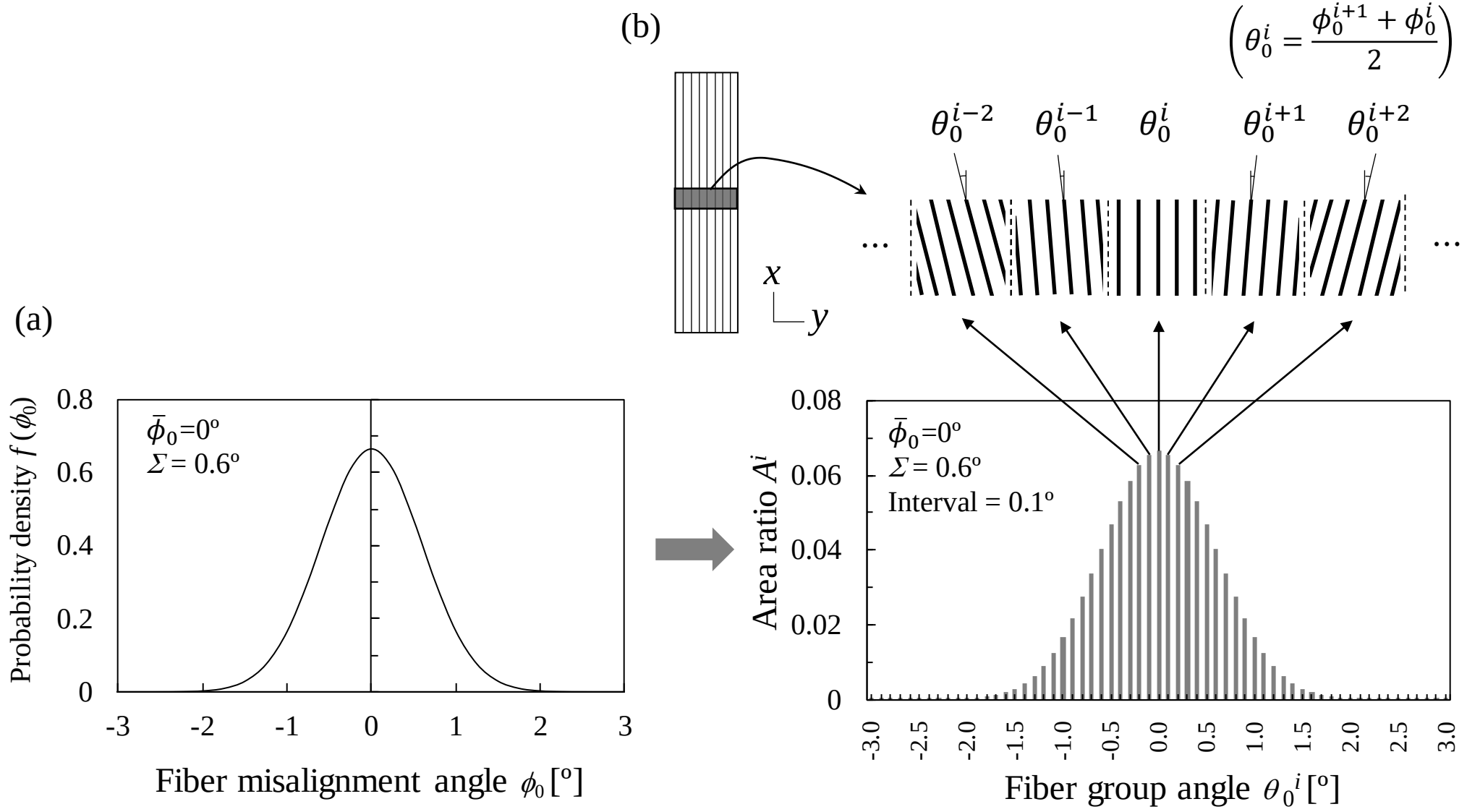

Figure 3 Experimental mechanical response of UD CFRP (T800S/#2592).
(a) Longitudinal shear stress-strain curves (b) Axial compressive stress-strain curves. The coefficients of variation are shown in parentheses.

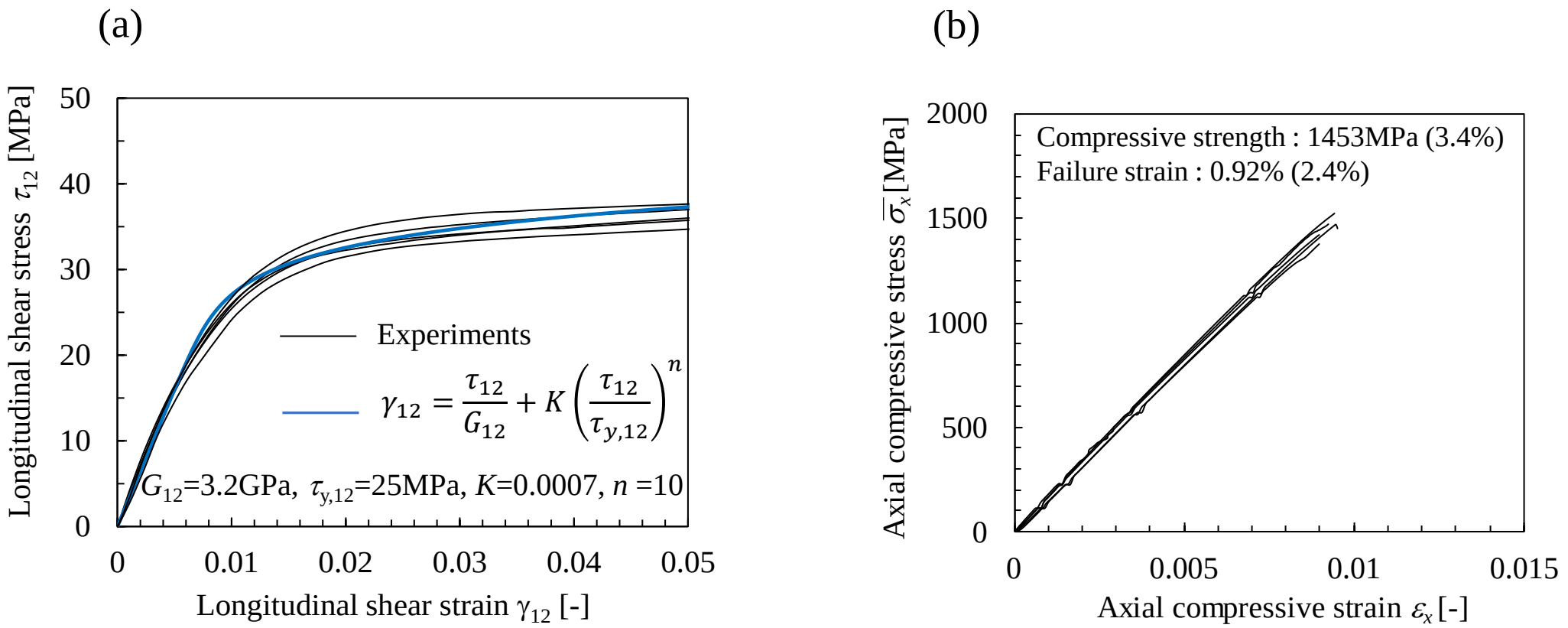

Figure 4 Analytical axial compressive stress-strain curves.
(a) Stress-strain curves assuming uniform fiber misalignment angle.
(b) Scaled stress-strain curves by using the area ratio and the resultant stress-strain curve of $\bar{\phi}_0 = 0^o$ and $\Sigma = 0.6^o$.

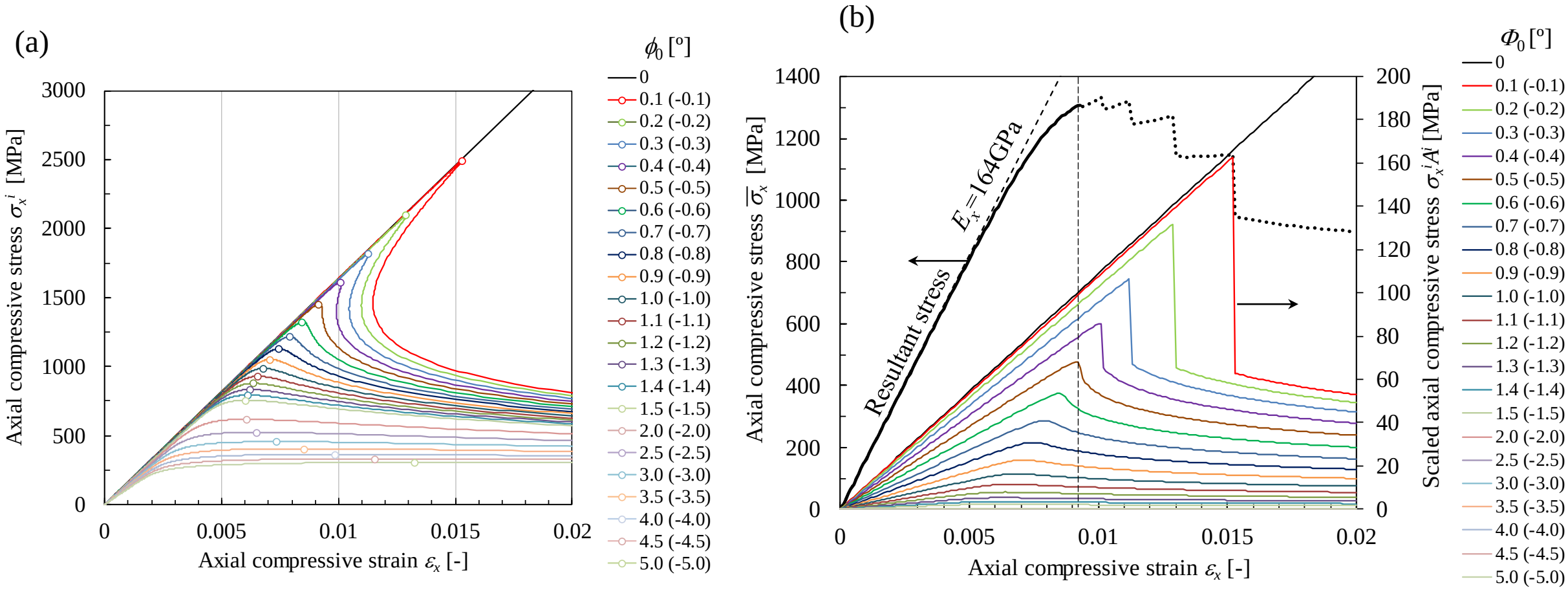

Figure 5 The effect of variability (standard deviation) of fiber misalignment angle.
(a) Probability density functions. (b) Axial compressive stress-strain curves.

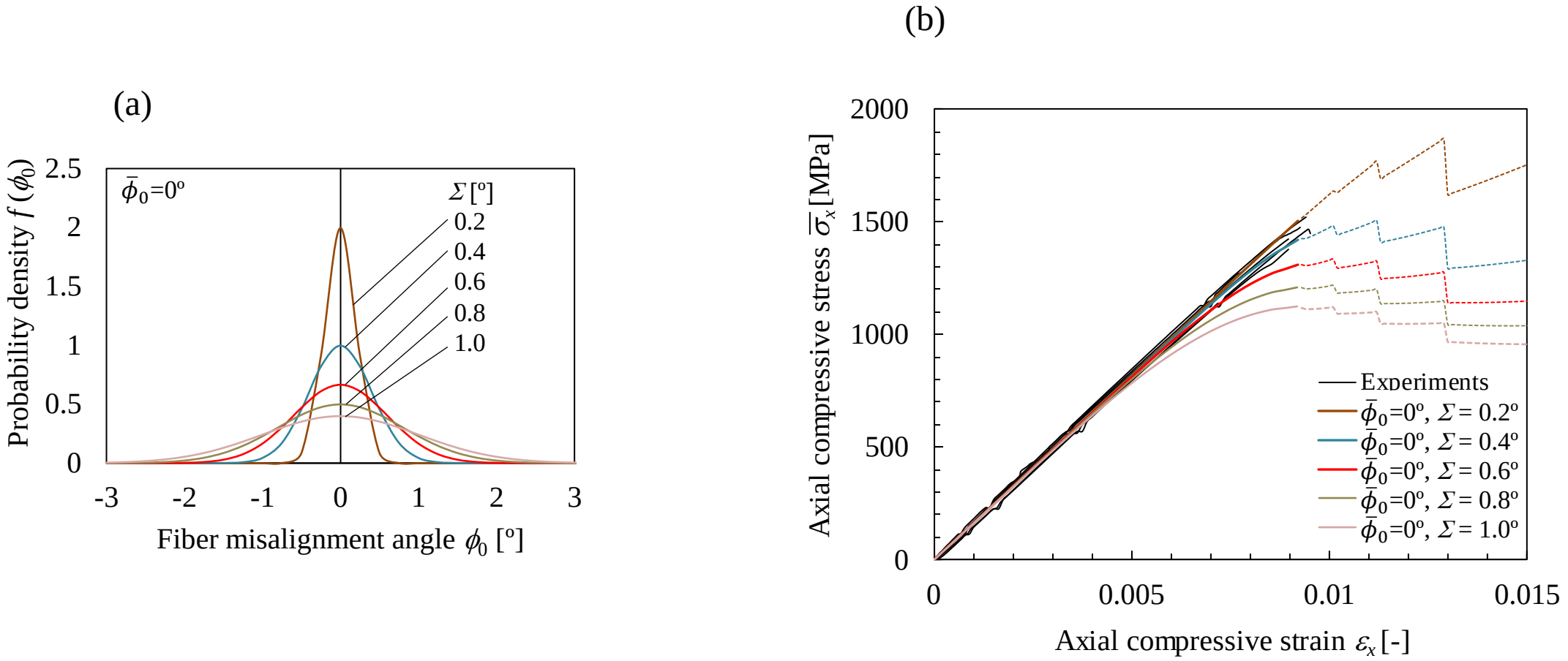

Figure 6 The effect of mean fiber misalignment angle.
(a) Probability density functions. (b) Axial compressive stress-strain curves.

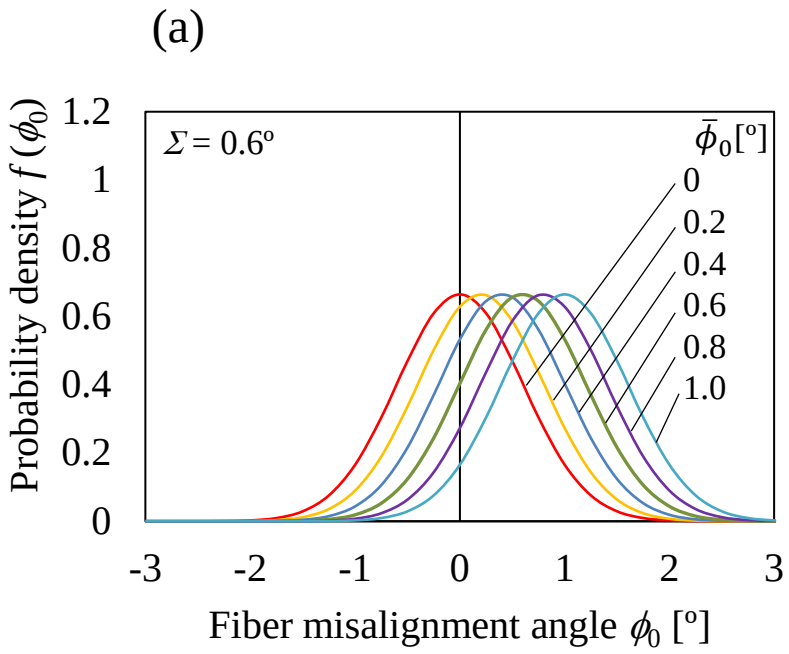

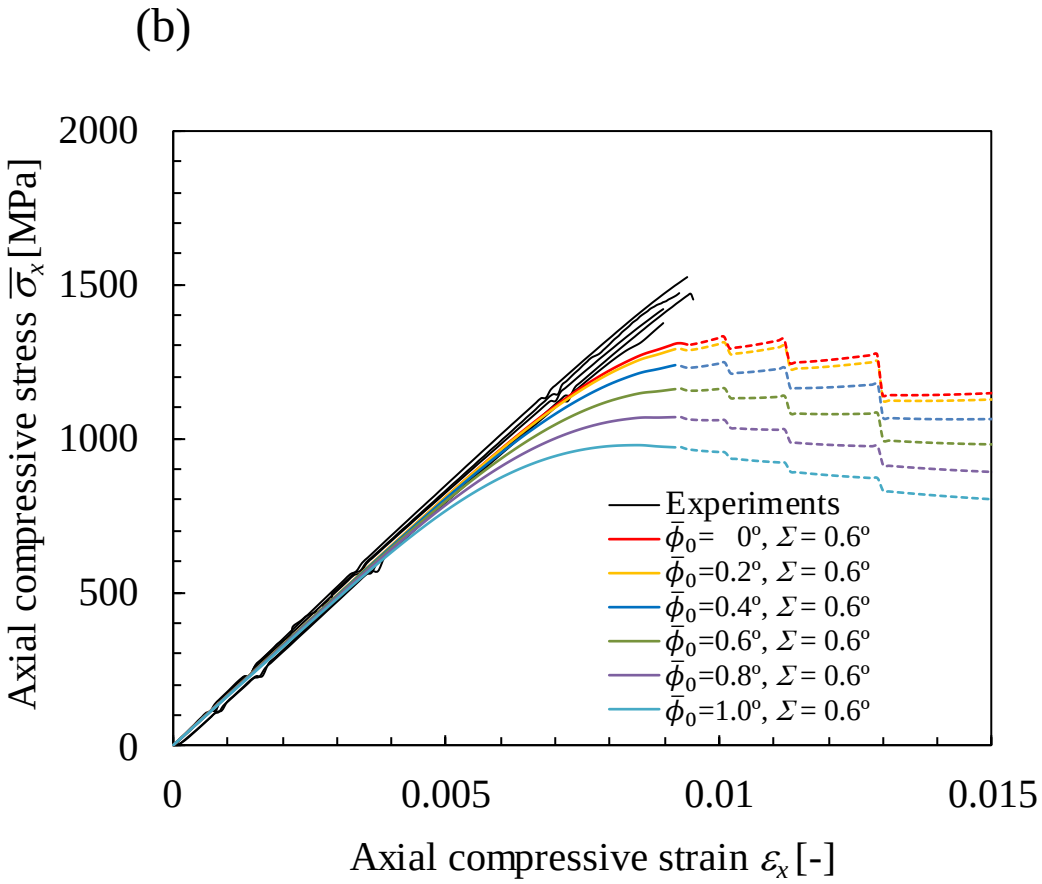

Figure 7 The combined effect of variability (standard deviation) and mean fiber misalignment angle on the axial compressive strength.

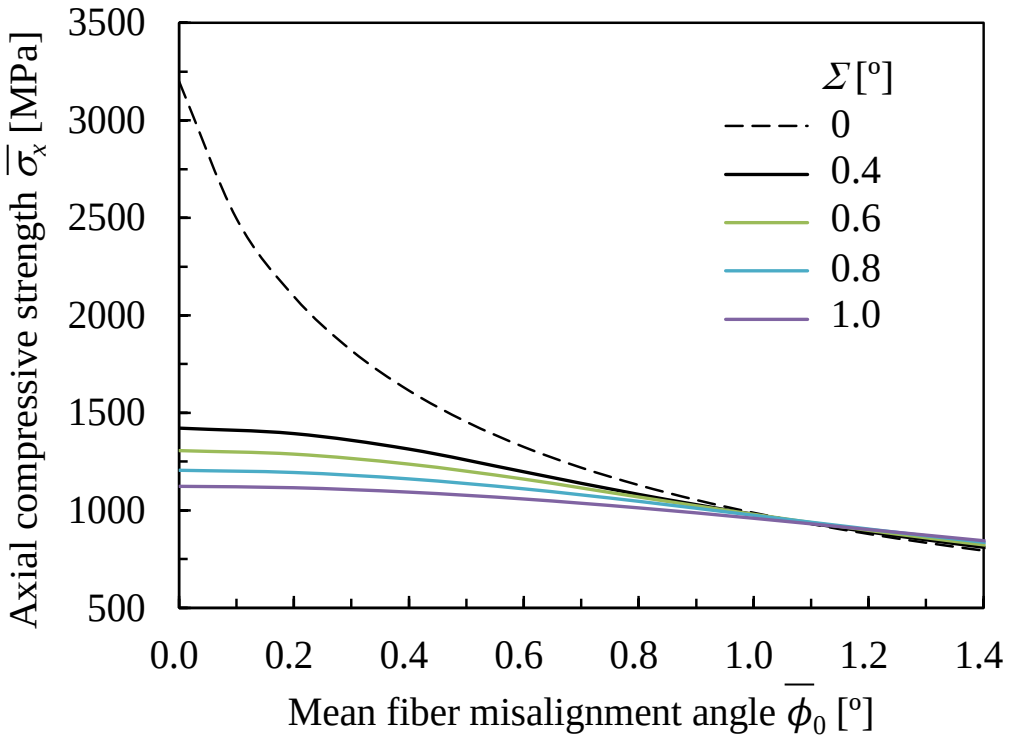

Figure 8 Determination of fiber kinking critical stress and kink-band width.

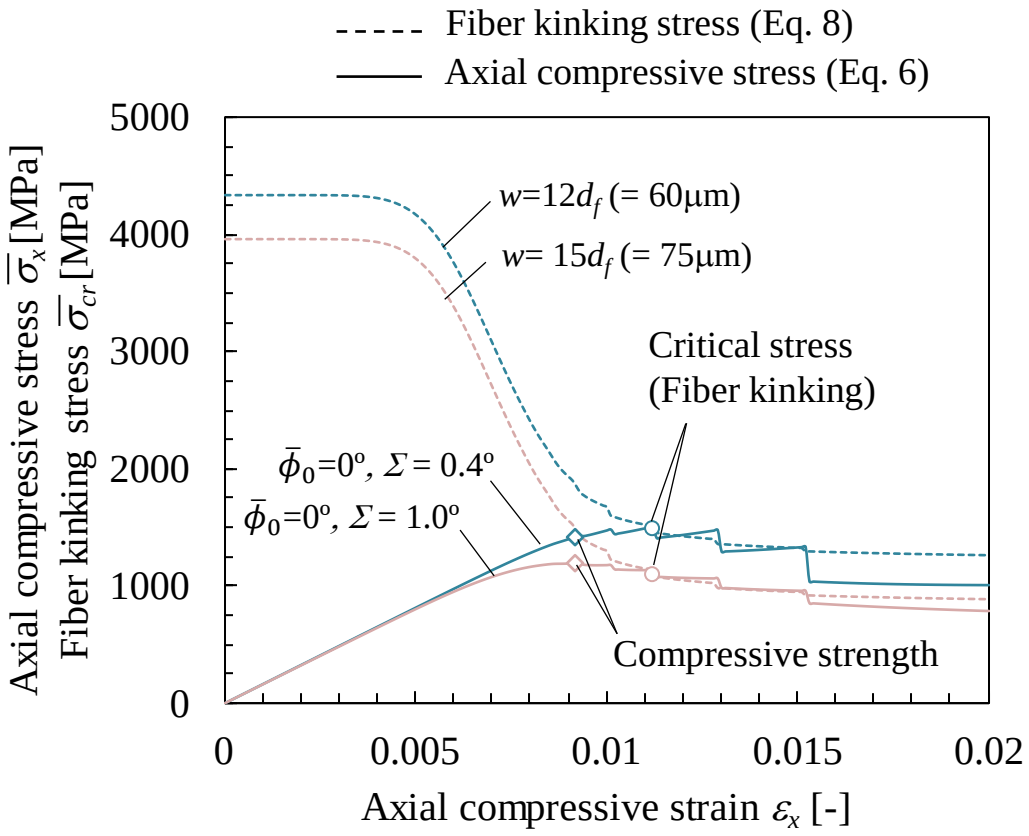

Table 1 Material properties used in the calculation of axial compressive behavior.

E_{11} [GPa]	E_{22} [GPa]	G_{12} [GPa]	ν_{12} [-]	V_f (V_f^{2D}) [-]	d_f [μm]
164	9.1	3.2	0.1	0.65 (0.72)	5
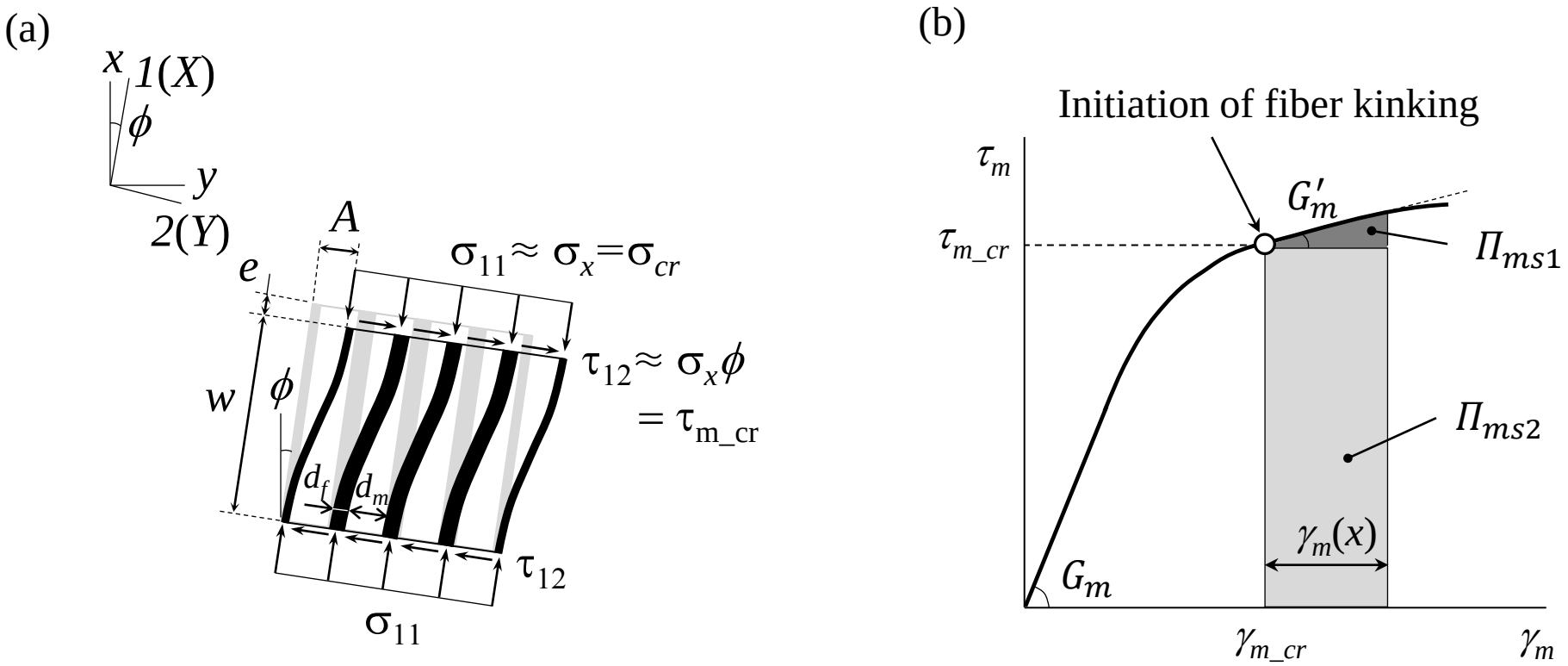
Figure A1 Fiber kinking deformation.
(a) Deformed shape before and after fiber kinking. The non-kinked shape shown in light gray.
(b) Strain energy of matrix per unit volume due to shear deformation.